PHOTOMASK

BACUS—The international technical group of SPIE dedicated to the advancement of photomask technology.

Investigation of stochastic roughness effects for nanoscale grating characterization with a stand-alone EUV spectrometer

Sven Glabisch, Sophia Schröder, and **Sascha Brose,** RWTH Aachen University TOS - Chair for Technology of Optical Systems, Aachen, 52074, Germany; JARA – Fundamentals of Future Information Technology, Jülich, 52425, Germany; **Henning Heiming,** RWTH Aachen University TOS - Chair for Technology of Optical Systems, Aachen, 52074, Germany; **Jochen Stollenwerk** and **Carlo Holly,** RWTH Aachen University TOS - Chair for Technology of Optical Systems, Aachen, 52074, Germany; JARA – Fundamentals of Future Information Technology, Jülich, 52425, Germany; Fraunhofer ILT - Institute for Laser Technology, Aachen, 52074, Germany

ABSTRACT

Fast and non-destructive non-imaging metrology of nanostructures is crucial for the development of integrated circuits and for the corresponding in-situ metrology within fabrication processes. Stochastic variations related to the gratings local period (line edge roughness, LER) and line width (line width roughness, LWR) are of special interest due to their key role in the minimal achievable structure size. Non-imaging metrology approaches taking these statistic variations into account are quite limited. For scatterometry, models predict a change in the grating's diffraction efficiency according to a Debye-Waller factor but only in the non-zeroth diffraction orders. The authors perform simulations of nanoscale gratings that suggest an influence of LER and LWR on the reflectance (zeroth diffraction order efficiency) which motivate an extended study on LER and LWR measured by spectrally resolved EUV reflectometry here described as EUV spectrometry. The authors present reconstruction results of nanoscale gratings measured with a compact spectrometer utilizing extreme ultraviolet (EUV) radiation emitted by a discharged-produced plasma (DPP) EUV source. The use of two sequential spectrographs, one for the reference measurement of the source spectrum, and the other one for the measurement of the spectrum after sample interaction, combined within the experimental setup allow measuring the broadband reflectance with 2% relative uncertainty of samples under various grazing incidence angles. The method offers a proven sub-nm reconstruction accuracy for critical grating parameters. Within the presented study, the measured samples are dedicated test samples, fabricated to

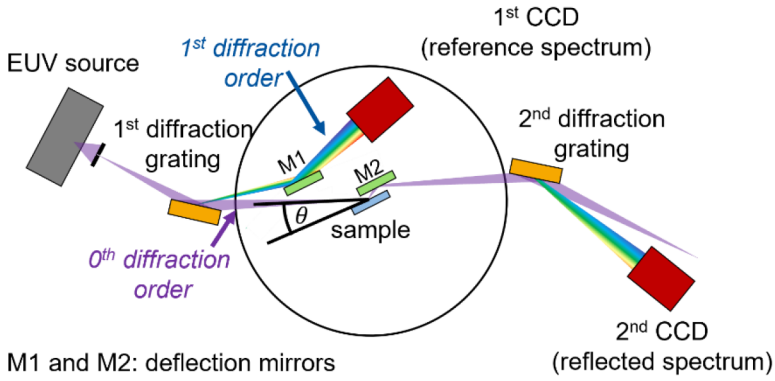

Figure 1. Schematic representation of the EUV spectrometer realized at RWTH-TOS. The EUV source emits unpolarized broadband emission of a xenon gas discharge. The EUV radiation is directed onto a first diffraction grating and the spectrally resolved first diffraction order is captured by an in-vacuum CCD camera (reference spectrum). The zeroth diffraction order interacts with the sample before the radiation is redirected to a second diffraction grating, spectrally resolved and captured again by a second CCD camera (reflected spectrum).

BACUS NEWS

NOVEMBER 2022
VOLUME 38, ISSUE 11

SPIE.

12293-30

EDITORIAL

(P)awsome tech trends!

Vidya Vaenkatesan, ASML Netherlands BV

The recently concluded SPIE Photomask and EUV Lithography 2022 conference, with over 550 attendees and 90 presentations, including an engaging panel discussion, was a roaring success. The conference had interesting plenary sessions on the future of semiconductor technology, and sustainable computing luminaries from Intel, Hoya Corp., Applied Materials, and IBM Research.

2022 marked yet another great initiative by SPIE Photomask to organize quarterly free webinars wherein industry stalwarts will talk on a wide range of topics relevant to the semiconductor mask industry outside the confines of a conference. This would make cutting-edge technology presentations accessible to all.

The semiconductor market is set to grow from USD 590 billion in 2022 to 1065 billion-worth USD in 2030 (The semiconductor decade: A trillion-dollar industry | McKinsey). Seventy percent of this growth is predicted to be driven by just three industries: automotive, computation & data storage, and wireless technology. To meet this projected demand, our industry has plenty of challenges in the coming years – be it from equipment suppliers, mask makers, designers, or the material industry.

Talking about the semiconductor market and particularly the wireless segment, the recent trend of the smart watch with so many features to track health parameters, along with the intelligence to call for help in case of a crash or fall, is a remarkable application of wireless technology. Intrigued by this, the projected growth of wireless communication, and my two adoring Labrador Retrievers, I started to think about technology and its applications in the pet world! I learned of an RFID-based product that reads the chip on a cat and allows them to enter their homes. Since the reader is located on the outside flap, only the right cat can enter and any animal can exit. I was truly impressed with this simple application of ubiquitous technology in human space.

Piqued by this knowledge, I looked up the pet tech market size and trends. The market surpassed USD 5 billion in 2021 and is set to grow at around 20% CAGR from 2022 to 2028. The market witnessed steady growth in 2021 owing to the pet humanization trend, an increase in pet adoption rates, and high demand for advanced products and services for pet owners. The sectors demand automatic solutions that require less attention from the owner and provide effective monitoring and tracking data remotely. Apparently, the growing prevalence of obesity in pets will encourage owners to purchase intelligent pet-tech products and monitor their health parameters such as breathing, sleep, and heart rate. Pet-tech products will also support pet owners in achieving daily activity goals to maintain their pet's fitness.

Now, how different is that from what we are building for our own health monitoring? It felt reassuringly comfortable to know that my furry friends' wellbeing is also part of the overall growth of the semiconductor technology and market. For further reading, Pet Tech Market Size, Statistics - Industry Share Report 2028 (gminsights.com)

On that "woofy" note, I wish you all a healthy and productive remaining 2022!

BACUS

N • E • W • S

BACUS News is published monthly by SPIE for *BACUS*, the international technical group of SPIE dedicated to the advancement of photomask technology.

Managing Editor/Graphics Linda DeLano
SPIE Sales Representative, Exhibitions, and Sponsorships Melissa Valum
BACUS Technical Group Manager Tim Lamkins

SPIE.

P.O. Box 10, Bellingham, WA 98227-0010 USA
Tel: +1 360 676 3290
Fax: +1 360 647 1445
SPIE.org
help@spie.org

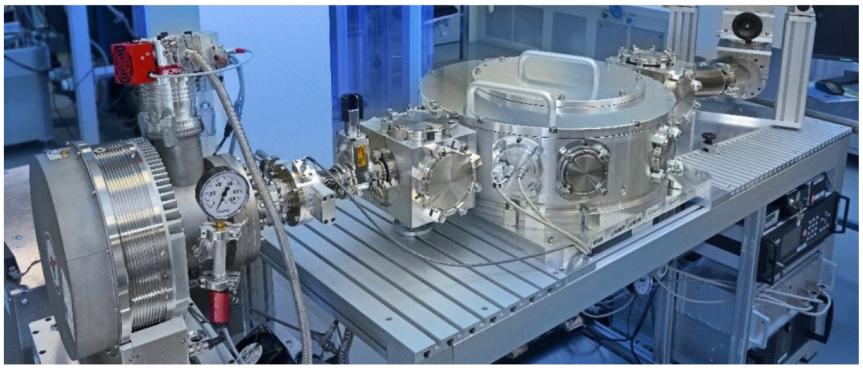

Figure 2. Photograph of the EUV spectrometer in the RWTH-TOS cleanroom environment (footprint 1 x 2.5 m²).

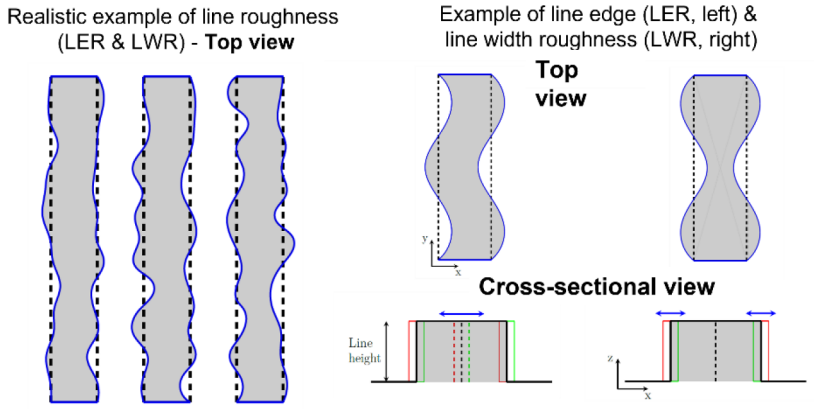

Figure 3. Schematic representation of three realistic grating lines (left schematics) with randomly distributed line edge and line width roughness. Schematic representation of line edge and line width roughness (right schematics) for a periodic distribution of the line edge position and line width position in the top view of a single grating line (top) and in the cross-sectional view (bottom). Periodic roughness is a special case but can provide a comparable effect on the diffraction efficiency discussed in detail by a. Kato et al.[7].

exhibit well-defined LER and LWR at different grating periods and line widths. In addition, the samples are also cross-characterized by the Physikalisch-Technische Bundesanstalt (PTB, Berlin). Experimental and simulative results are discussed to derive approaches to include LER and LWR as parameters in the physical model for reconstruction.

1. Introduction

Functional structures of integrated circuits are shrinking and getting more complex for decades. This development was enabled due to the huge progress of lithographic fabrication techniques as well as the corresponding measurement techniques. In recent years, lithography utilizing EUV radiation gains importance for high-volume manufacturing of integrated circuits reaching the highest resolution so far1. To achieve the required quality and reliability of the fabrication process, several quality control steps are integrated within the process (in-line) or are carried out regularly independent from the fabrication (offline)[2]. For this purpose, dedicated test fields are manufactured next to the functional parts on a wafer during the process and characterized to extract information on the process quality of the actual functional structures of the device[3,4].

These test fields are typical nanoscale gratings, consisting of periodic lines and spaces to provide high sensitivity for radiation-based measurement techniques due to interference effects, with comparable dimensions like the integrated circuit under manufacture[3].

Characterization techniques for these test fields have to deliver information on the geometrical properties as well as its compositional cross-section and need to be fast and non-destructive in order to be included within the fabrication process which limits the selection of suitable techniques mostly to non-imaging techniques based on scattered radiation[4]. Due to the large spot size (test field size ≈ 50 µm x 50 µm) of these measurement techniques compared to typical dimensions of the utilized test structure (≈ 10 nm – 100 nm), these techniques provide averaged information of the structures within the measurement spot but local features like defects remain undetected[3]. Two features of special interest are stochastic properties of the nanoscale gratings period along the grating line, namely line edge roughness (LER), and the line width, namely line width roughness (LWR), because they are a key limitation factor to the minimal achievable feature size of the lithographic process[5].

Due to the averaging nature of radiation-based measurement techniques, their feasibility to extract stochastic information of the test fields geometrical features is not generally given. Techniques capable to characterize LER and/or LWR are for example grazing incidence small angle X-ray scattering (GISAXS) which relies on measuring the diffraction efficiency of multiple (zeroth and non-zeroth) diffraction orders and modelling the influence of LER/LWR based on a damping term delivered by theory[4]. The derivation of this damping term, typically called Debye-Waller factor (DWF), is based on the variation of the grating period respectively line width of a perfect binary grating with independent variation of the corresponding grating parameter and does not propose

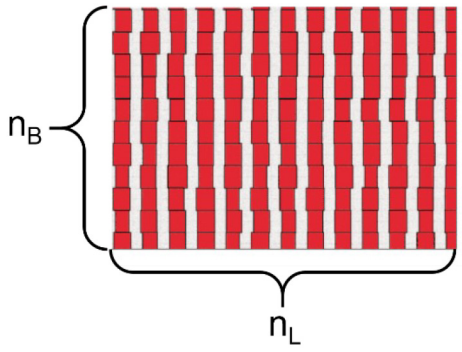

Figure 4. Layout of the unit cell for investigations of a computationally efficient simulation setup. Image adapted from A. F. Herrero et al.[6].

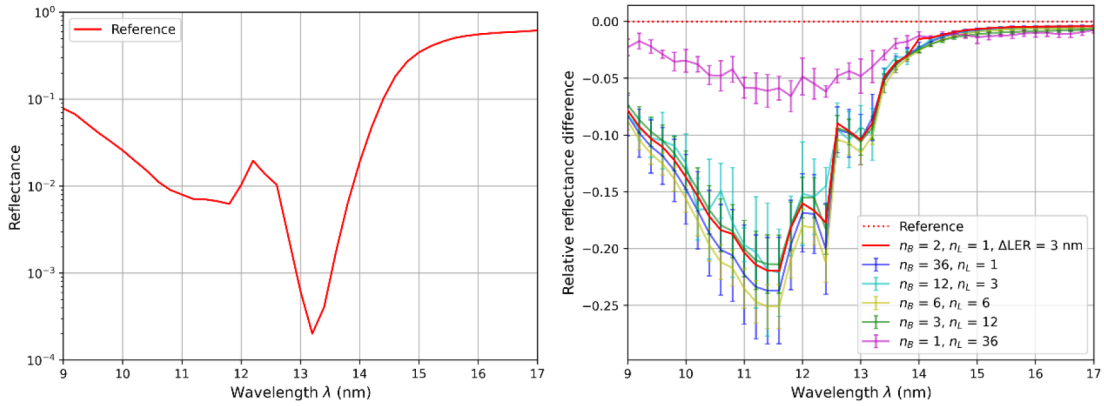

Figure 5. Reflectance of the simulated grating on the left for a grating incidence angle of 6°. The reference is simulated without any roughness. Comparison of the influence of the line and block distribution for a σ_{LER} of 3 nm within a unit cell consisting of n_L lines separated in n_B blocks on the right.

an influence on the zeroth diffraction order efficiency[6,7].

In this paper, the influence of stochastic properties of a nanoscale grating on the zeroth diffraction order efficiency is investigated in a simulative approach serving as a basis for measurements and reconstructions of three dedicated and cross characterized test samples with defined LER and LWR. The simulative studies are carried out with two different Maxwell solver, namely Dr. Litho and JCMsuite[17,18,19], to achieve a framework for fast and accurate simulations of nanoscale gratings considering stochastic properties.

2. EUV Spectrometry

In this work, EUV spectrometry is applied and evaluated to investigate nanoscale gratings with dedicated LER and LWR properties. EUV spectrometry measures the broadband reflectance of the sample under investigation for various grazing incidence angles, which corresponds to measuring the zeroth diffraction order efficiency of a grating-like sample[8,9]. Based on the reflectance data, several surface-related geometrical features as well as sub-surface cross-sectional information and material specification can be reconstructed in a model-based approach with up to sub-nanometer accuracy in terms of averaged properties of the sample[8,9]. Besides grating-like samples, the utilized technique is suitable for the reconstruction of thin layer systems and its capability for the determination of optical constants[10] with an absolute uncertainty below 0.001 has been demonstrated[10]. This approach is comparable to established techniques and mainly differs by the utilized wavelengths. An advantage of utilizing EUV radiation is its strong absorption in any matter in combination with element-specific absorption edges of relevant materials (e.g. Si-L absorption edge at ≈ 12.4 nm wavelength[11]), which results in a high material contrast and therefore a high sensitivity regarding the analysis of the material composition[12].

To measure the spectral and angular resolved reflectance of the samples, the compact EUV spectrometer, developed at the Chair for Technology of Optical Systems, RWTH Aachen University (RWTH-TOS)[8,9,10], shown in Figure 1 & Figure 2 is utilized which main components are the radiation source, two sequential spectrographs, and the sample positioning system. Due to the strong absorption of EUV radiation, the whole setup is operated under vacuum conditions, reaching pressures below $5{\cdot}10^{-6}$ mbar at the sample position. A discharge-produced plasma (DPP) EUV source emits unpolarized broadband EUV radiation from a hot and dense xenon plasma with high intensity in a spectral range from 10.7 nm – 15.5 nm[8] and with reduced intensity up to 20 nm. The beam is spatially filtered by an aperture and the non-EUV part of the spectrum is spectrally filtered out by a 200 nm thick zirconium thin film filter before the beam is directed to a first diffraction grating that is illuminated in classical configuration (beam perpendicular to grating lines). Afterward, the spectrally resolved first diffraction order of the probing beam is directed towards a CCD camera which captures the so-called reference spectrum. The zeroth diffraction order can further propagate and is also spatially filtered by an aperture to achieve vertical beam dimensions down to 50 µm before the beam hits the sample under investigation. After sample interaction, the beam is deflected by a movable and rotatable mirror to enable a fixed exit position out of the sample chamber even when the sample is illuminated under various grazing incidence angles. A second spectrograph is placed behind the sample and captures the spectrum

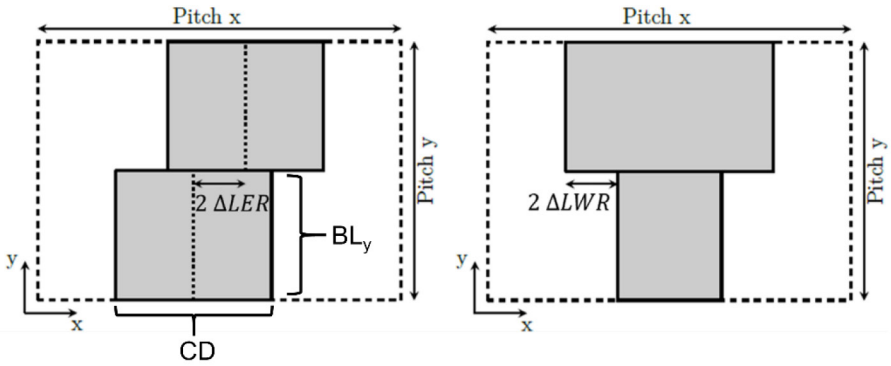

Figure 6. Unit cell of the simplified simulation approach in top view for line edge roughness (left) and line width roughness (right) according to the parameter Δ_{LER} respectively Δ_{LWR}. The pitch x corresponds to the period of the grating under simulation while the pitch y is orientated along the grating line.

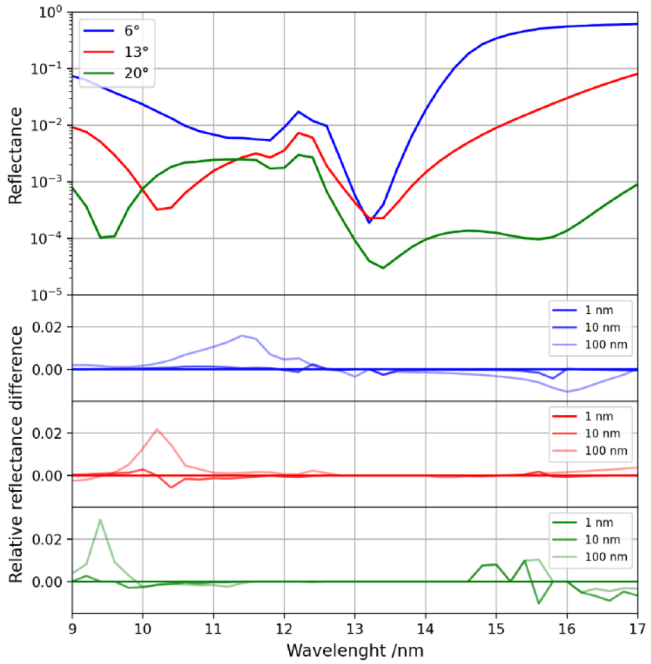

Figure 7. Influence of the period of a grating's unit cell along the grating lines pitch$_y$ (see Figure 6, corresponding to 2·BL$_y$) for different angles and wavelengths. Differences in the reflectance (relative to 1 nm period simulation) are usually below 2%. A possible explanation could be an insufficient number of Fourier orders for the transformation of the grating structure within the Dr. Litho approach. In the following simulations, a pitchy in the y-direction (along the grating lines) of 10 nm is chosen.

after radiation-sample-interaction (reflected spectrum). This way, naturally occurring fluctuations of the emitted spectrum are monitored pulse by pulse. In addition to the consideration of the source fluctuations, the influence of all other optical components on the reflectance signal needs to be considered. For this purpose, an additional measurement of a sample with well-known reflectance (characterized by Physikalisch-Technische Bundesanstalt, PTB) is performed which allows determining the combined influence of the mirrors and gratings, considered during the evaluation of the unknown sample's reflectance[9,10,13]. The sample itself is placed on a 6-axis manipulator for alignment and is placed on an additional stage to rotate the sample-mirror pair in order to capture the angular dependency of the reflectance spectrum.

With the current setup, the angle can be adjusted between 5° and 30° grazing incidence angle relative to the sample surface[10]. Due to the relatively low source emission between 15.5 nm and 20 nm and a resulting lower signal-to-noise ratio of the recorded spectra, the spectral range for the reconstruction of the sample parameters is typically limited to the high-quality range from 11 nm to 15 nm. The same argument is valid for a limitation of the angular range within the reconstruction process due to a low reflectance of some samples with increasing grazing incidence angles and the accompanying lower signal-to-noise ratio. Previous investigations have demonstrated that measurements conducted with the compact EUV spectrometer achieve a relative uncertainty on the absolute reflectance value of below 2% for an angular range below 15° grazing incidence angle[13]. The relative uncertainty for higher angles is increased due to the already mentioned reduced signal-to-noise ratio but also due to polarization-specific reflectance values of each optical component and the increase of this effects for higher angles.

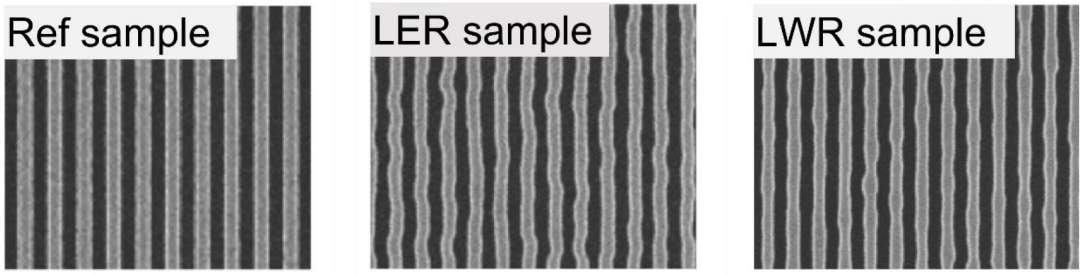

Figure 8. Top-down SEM of the measured samples without a designed roughness (Ref), with designed line edge roughness (LER) and designed line width roughness (LWR). Images adapted from A. F. Herrero et al.[6].

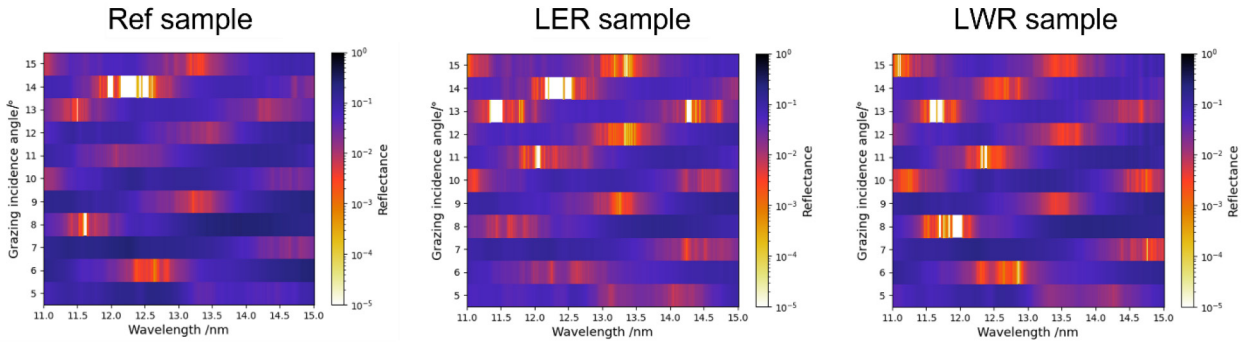

Figure 9. Measured reflectance of the three samples. The reflectance of all three samples provides a comparable signature across the measurement range. Major differences are related to the exact position and intensity of an interference maxima/minima e.g. Ref, LER, LWR at a 5° grazing incidence angle.

3. Line Roughness in Theory and Computational

Manufactured nanoscale gratings exhibit imperfections of different natures, independent from the utilized fabrication process. On the one hand, these imperfections can be local and only occur at specific positions on the sample, e.g. by the deposition of contaminations or due to the manufacturing process itself[4]. On the other hand, statistical processes like the absorption of photons within the resist during exposure or the quantization of photons cause variations of the lithographic process quality over the whole exposed area[4]. These statistical effects and their resulting influence on the final grating pattern are typically considered roughness parameters. The two main parameters for roughness in the field of nanoscale grating characterization are the so-called line edge roughness (LER) and line width roughness (LWR) which describe the statistics for variations of the line mean position with a constant line width (LER) or respectively a variation of the line width (LWR) along the grating lines[6,14,15]. Both effects are schematically shown for a random (combined) and periodic distribution in Figure 3. For this purpose, the parameters σLER and σLWR are introduced which describe the standard deviation with respect to their nominal line position or respectively line width. It should be mentioned at this point, that several definitions of LER and LWR exist and a non-neglectable part of the literature uses 3·σLER respectively 3·σLWR as the definition for LER and LWR and care should be taken comparing the literature.

Due to the importance of LER and LWR with respect to the minimal achievable feature size, LER/LWR effects are discussed for several years and different approaches to consider the corresponding effects are considered in theory as well as validated experimentally[4,6,7,14,15]. A detailed derivation of an analytic expression can be found in A. Kato et al.[16] for a gaussian distribution of the line mean position and the line width. The resulting analytic expression is given in equation 1 (gaussian distribution[6]) but it requires some approximations.

$$I_{Roughness}(q_x) = I_{Ideal}(q_x) \cdot exp\,(-\xi^2 \cdot q_x^2) \quad (1)$$

with I_{Ideal} the intensity of an identical but non-rough grating, $I_{Roughness}$ the intensity considering the roughness, q_x the momentum transfer in reciprocal space according to equation 3 and ξ the effective roughness considering the uncorrelated and combined roughness attributed to LER and LWR. Besides of approximations regarding the distribution of LER and LWR, the equation considers an infinite periodic, perfect binary grating according to equation 2 with a small displacement/width variation of the grating lines. The resulting analytic expression in equation 1 consists of a term IIdeal for a perfect grating without LER or LWR and an exponential damping term called Debye-Waller-factor (DWF) or a Bessel-function like damping term, here shown for the case of LER but besides of a constant factor, the same term is delivered for LWR[7]. The damping factor depends on the diffraction order m, the period length of the grating structure, the grazing incidence angle θ relative to the sample surface, and the azimuthal angle ϕ with ϕ = 0° corresponding to an illumination along the grating lines. The indices "in" and "out" indicate the incoming respectively outgoing beam. Several publications following this approach for scatterometry, e.g. Grazing-Incidence Small-Angle X-ray Scattering (GISAXS) validated its feasibility to model LER and LWR based on the intensity damping on higher diffraction orders[4,6] but for the reflectance (zeroth diffraction order, m = 0) no influence due to LER or LWR is proposed. In good scientific practice, this assumption needs to be validated as well, which motivates a simulative study of LER and LWR effects on the zeroth diffraction order. For this purpose, primary simulative investigations are carried out to determine the optimal simulative layout which provides a high accuracy while keeping the required time per simulation as short as possible.

The primary investigations are conducted on a simplified grating consisting of silicon with a period length P of 120 nm perpendicular to the grating lines, a line height H of 35 nm, a line width (CD) in the x-

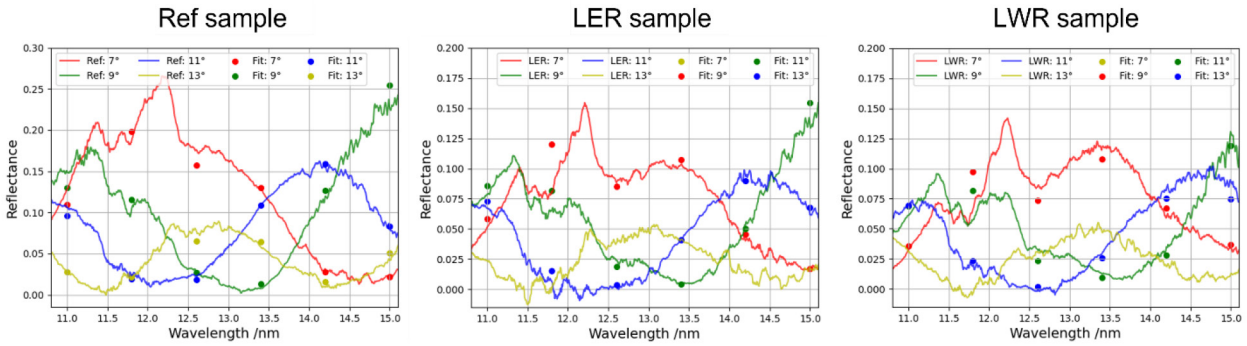

Figure 10. Results of the fitting process (fit results as dots) for all three samples plotted against the measurements (solid line): Most of the fitted reflectance values are in good agreement and the overall curvature of the measurement is well reproduced by the fit.

Table 1. Comparison of the determined grating parameters by both facilities. PTB performed GISAXS measurements at the BESSY II synchrotron, RWTH-TOS performed EUV spectrometry [4,15]. Deviations of these amplitudes might be caused by multimodalities that are not good enough resolved within the Bayesian optimization process.

	Ref			LER			LWR		
Facility	**PTB[4,15]**		**RWTH-TOS**	**PTB[4]**		**RWTH-TOS**	**PTB[4]**		**RWTH-TOS**
Line height H /nm	119.5 ± 0.1		118.6	121.3 ± 0.3		119.4	122.9		120.9
Silicon CD at half height (corrected) /nm	67.3 ± 0.3		65.2	64.9 ± 1.2		64.6	64.6		63.7
Sidewall angle α /°	5.3 ± 0.3		7	6.1 ± 0.6		6.4	4.4		5.7
Oxide thickness H_{SiO2} /nm	3.9		7.7	not determined		4.8	not determined		4.1
ΔLER /nm	SEM 2.2	DWF 1.9 ± 0.1	1.8	SEM 6.4	DWF 5.1 ± 0.1	4.3	SEM 3.6	DWF 3.1	3.0
ξ /nm									

direction of 50 nm (perpendicular to grating line) and a sidewall angle α of 0° (perfect rectangular grating). These parameters were chosen under consideration of the required computational time (scales with the size of the structure) but are realistic for typical but simple semiconductor test fields. Simulations of gratings with rectangular grating lines are carried out using the well-established Maxwell's equation solver Dr. Litho which provides a fast and semi-analytical approach[17,18].

A unit cell was chosen consisting of 36 blocks distributed among n_L lines, each separated within n_B blocks according to Figure 4. The number of blocks in each line and the number of lines within the unit cell are varied while the total number of n_L x n_B remains constant (here n_L x n_B always equals 36) in order to investigate the influence of the block distribution. Each of these blocks exhibits a width of 5 nm in the y-direction (parallel to the grating line).

A modification of the nominal position of a block Δx_i, where i is the index of the block, corresponds to line edge roughness and is extracted out of a Gaussian distribution with an expectation value $\mu = 0$ and a standard deviation σ_{LER}. Similarly, the modification of a block ΔCD_i corresponding to line width roughness is also extracted out of a Gaussian distribution. It should be mentioned that the actual mean value and the distribution do not necessarily provide these properties due to the small number of blocks which contribute to the layout. Due to an influence of the actual values of ΔCD_i, respectively Δx_i, all simulations are carried out five times to provide an uncertainty related to the underlying Gaussian distribution. All simulations are performed for different grazing incidence angles θ (5° to 30°) and σ_{LER}, σ_{LWR} (0 nm to 5 nm) and exemplarily shown for θ = 6° and σ_{LER} = 3 nm in terms of the reflectance difference (subtracted from a simulation with σ_{LER} = 0 nm which means no line edge roughness) in Figure 5.

Most of the simulations are in agreement with the standard deviation related to the influence of the actual block distribution delivered by the multiple executions of the simulations (each block distribution is unique and extracted from a random gaussian distribution). All simulations show a comparable modulation from an ideal grating without roughness besides the layout consisting of lines without a segmentation along the line (n_L = 36, n_B = 1) where significantly different results are achieved. Here the line means the position of each grating line is shifted in accordance with the gaussian distribution of with σ_{LER} = 3 nm. A possible explanation could be the absence of classical diffraction which would occur due to a grating-like structure perpendicular to the illumination beam. The absence of a modification along a grating line might result in an underestimation of the intensity modulation introduced by diffraction-like behavior due to the line edge roughness. In addition to the first set of simulations, simulations utilizing a more simplified layout were performed which consist of only two blocks in a single line (see Figure 6). The simulation results (see n_L = 1, n_B = 2, ΔLER = 3) provide convincing agreement with the previous simulations within a one-sigma uncertainty related to the influence of the Gaussian distribution of the five simulations performed for each combination of n_L and n_B. The feasibility of this approach is surprising due to its simplicity, but no deviation is found during the simulative study

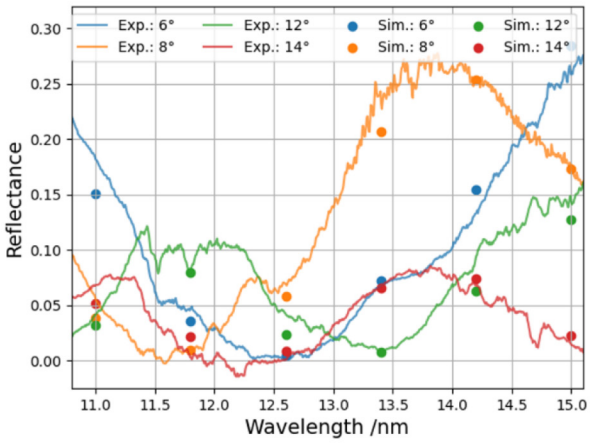

Figure 11. Comparison of the measured (Exp.) and calculated (Sim.) reflectance for the reference sample for angles not used during reconstruction. The overall good agreement provides additional trust in the reconstruction result.

that provides a restriction for this simplification. A reasonable explanation could be the presence of classical diffraction due to the displacement of the two blocks which provides a comparable intensity modification on average as a finer segmentation of the grating according to a Gaussian distribution. The shift (ΔLER) respectively the extension/compression (ΔLWR) of one of these blocks corresponds to standard deviation σ_{LER}, σ_{LWR} in the case of Gaussian distributed blocks. This approach provides the advantage, that only a single simulation needs to be carried out and no influence of the actual block distribution needs to be estimated. Among the investigated angles and line edge and width roughness values, no significant deviation for this approach was observed. Therefore, the following simulations are performed utilizing this simplified layout. It should be mentioned, that in accordance with most of the literature, only a difference in the amplitude of the modulation was found between simulations related to LER and LWR[16,15] which is caused due to correlation respectively anti-correlation of the line edge position considering LER and LWR. Due to this relation, the effective roughness parameter ξ is introduced which combines the effect of both roughness types but not the correlations[6]. In the following, only the ΔLER approach is chosen to model the effective roughness in the following reconstruction process and is compared to the effective line roughness ξ reconstructed by the reference methods.

In order to estimate the influence of the block length in the y-direction (BL_y, see Figure 6) along a grating line, three cases are investigated which correspond to a block length BL_y much smaller than the wavelength BLy = 0.5 nm, once with the width in the order of the wavelength BL_y = 5 nm and once with a much larger block BL_y = 50 nm. The remaining grating parameter was chosen similarly to those before (Period length = 120 nm, line width CD = 50 nm, line height H = 35 nm). The reflectance difference (to BL_y = 0.5 nm) is shown in Figure 7 for a simple unit cell according to Figure 6 with a large ΔLWR of 2.5 nm. Even with this large CD differences (10 nm), the influence of the block length BL_y along a grating line is only relatively small and only provides differences in the order of 2% for single wavelength–incidence angle combinations. The block length BL_y for the following simulations is kept constant at 5 nm which seems reasonable considering the primary investigation.

4. Measurement and Sample Reconstruction

In order to apply the simulative approach from section 3 to real samples, three dedicated test samples with defined LER and LWR are measured utilizing the EUV spectrometer introduced in section 2. The samples consist of silicon lines with a nominal height H of 120 nm, a period of 150 nm, and a CD at half height of 65 nm and were stored under ambient conditions between primary characterization by PTB and experiments conducted at RWTH-TOS[6]. These sample parameters differ from those of the grating of the primary investigation in section 3 and require more intense simulations due to the larger dimensions. It is assumed that the approach introduced before is still valid, as the parameters are in a comparable order of magnitude and the diffraction behavior does not differ. The first sample, called Ref, is fabricated without any intended roughness, the second sample, called LER, is fabricated with an intended line edge roughness of $\max(x_j)$ = 5 nm, and the third sample with a line width roughness of $\max(\Delta CD_j)$ = 10 nm. Details of the sample's fabrication process and the utilized characterization techniques can be found at A. F. Herrero et al.[6]. It should be mentioned that A.F. Herrero et al.[6] characterized the line edge displacement distribution by scanning electron microscopy (SEM) and detected a Gaussian distribution. A top-down SEM image of the samples is shown in Figure 8 and provides a first guess of the fabrication process quality and a visualization of the differences between the LER and LWR samples. The measured effective roughness ξ values of the SEM characterization are given in Table 1 and are compared to those reconstructed using the measurements of GISAXS (PTB) and EUV spectroscopy (RWTH-TOS).

The azimuthal angle (ϕ = 0 corresponds to conical mounting) of the sample was aligned based on the symmetry of the sample's reflectance under rotation.

Figure 9 shows the measured reflectance of the three samples. The overall comparison shows a comparable reflectance for all three samples including the position of the destructive and constructive inference maxima/minima in the wavelength–grazing incidence angle space. This is reasonable due to the similar fabrication process with an electron beam lithography tool and the same, well controlled, etching process which results in a similar nominal parameter of the gratings. The fabrication process was optimized to achieve a low surface and height roughness providing sufficient overall homogeneity[6]. As shown by A. F. Herrero[6] in the primary characterization of these gratings, small deviations of the actual grating parameters between the Ref, LER, and LWR samples are in the order of 3 nm for the CD and the line height (compare Table 1).

The simulations for this study are carried out using the well-established Maxwell's equation solver JCMsuite[17,19] which provides a high degree of freedom regarding the geometrical layout of the structure under simulation. The use of a finite element method (FEM) based Maxwell solver enabled to include the sidewall angle α as an additional parameter. Silicon is known to suffer from oxidation under ambient conditions, therefore a homogeneous oxide layer across the grating structure was assumed and integrated as a reconstruction parameter. The low photon flux in the destructive inference minima of the reflectance of the sample provides

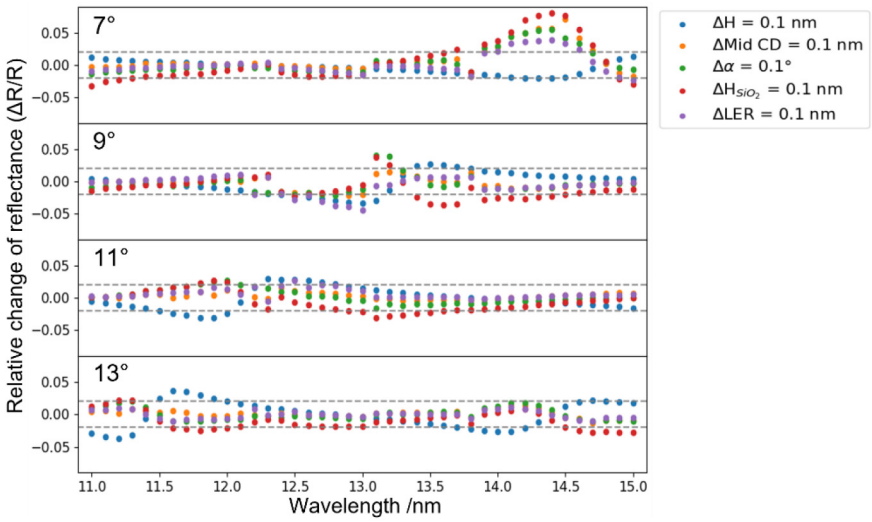

Figure 12. Relative reflectance change of the reference sample for the reconstructed grating geometry (see Table 1). Each parameter variation provides a unique signature enabling to distinguish between each parameter during the reconstruction. For specific wavelength–angle combinations, the relative change of reflectance exceeds the typical measurement uncertainty of 2% (dashed line) even for minor parameter changes of 0.1 nm respectively 0.1°. A proper choice of the wavelengths and angles included in the reconstruction process can increase the sensitivity for those parameters.

a low signal-to-noise ratio, leading to some numerical problems during the sample's parameter reconstruction. Reflectance regions with absolute reflectance values below 1% in combination with an approximately 2% relative uncertainty across the measurement range can be problematic during optimization. Therefore, an additional absolute uncertainty of 0.0005 was introduced to avoid overweighting during optimization based on a χ^2 function. The optimization process is carried out using the mentioned considerations with a Bayesian Optimizer provided by JCMsuite considering four angles (7°, 9°, 11°, 13°) at six wavelengths (11 nm to 15 nm in 0.8 nm wavelength steps) for unpolarized radiation, to compromise with the computational time. The results of the optimization are shown in Figure 10 for each of the three samples. Fit results and measurement curves are in good agreement in terms of intensity and curvature for each of the three samples. A higher disagreement at 11.8 nm at 7° and 9° for each measurement is visible which may be caused by a systematic error during measurement (e.g. straylight or the influence of higher diffraction orders).

For the comparison between the reconstructed parameters by PTB and RWTH-TOS, the line width reconstructed by RWTH-TOS needs to be corrected by the consumption of silicon due to the oxidation process. This correction considers, that 46% of the silicon dioxide layer thickness was original silicon before oxidation[20]. Table 1 compares the reconstructed values by both facilities. PTB determined the effective roughness parameter ξ once based on a Debye-Waller-factor (DWF) out-of-grazing incidence small angle X-ray scattering (GISAXS) measurements and validated this by SEM characterization. All values are in good agreement for each of the samples. In particular, the reconstructed parameter based on the RWTH-TOS approach ΔLER, which corresponds to the standard deviation of the effective roughness ξ is in very well agreement.

For the Ref sample, the oxide layer thickness reconstructed by RWTH-TOS exhibits the strongest deviation of all parameters in comparison to the previous characterization, partly explained by continuously present oxidation but this argument would also need to be applied for the LER and LWR samples where the reconstructed oxide thicknesses are in better agreement. A reasonable explanation is the presence of multimodalities, different solutions to the ill-posed reconstruction process of equal quality (comparable χ^2). The origin of this deviation is not completely clear and needs to be further investigated with an evaluation process suitable to reconstruct multimodalities for example a Markov Chain Monte Carlo (MCMC) approach. Due to the high computational cost, this evaluation was not conducted within the scope of this investigation but will be addressed in future investigations.

In order to validate the reconstruction results, additional simulations of the reflectance are carried out, exemplary as shown in Figure 11, for angles not considered during the optimization which also show a convincing agreement. This cross-check validates the reconstruction results.

Lastly, the sensitivity of the measured reflectance under parameter variation is simulated. This way a rough estimate of the expected uncertainty of the reconstructed parameters can be given assuming a change in the reflectance above the measurement uncertainty is distinguishable in the reconstruction process. Figure 12 exemplary shows the relative change of reflectance for a parameter variation of 0.1 nm respectively 0.1° for the Ref sample. It should be mentioned that simplified estimations on uncertainties need to be considered with caution, e.g. because they do not consider parameter correlations or multimodalities which require a high computational effort to resolve. Nevertheless, relative reflectance modifications of up to 5% are visible for each parameter including the roughness parameter ΔLER. In particular, anglewavelength combinations of constructive or destructive interference provide a strong variation due to roughness effects, probably caused by perturbated interference conditions. This observation provides promising insights into the feasibility of EUV spectrometry for the investigation of the effective line edge roughness.

5. Conclusion

In this work, the capability of a compact EUV spectrometer for the characterization of stochastic line roughness effects assigned to line edge and line width roughness is investigated. For this purpose, a framework to simulate the effect of line edge and line width roughness on the zeroth diffraction order of spectrally and angular resolved reflectance spectra of nanoscale gratings is tested. As a result of the simulative studies, it was demonstrated that it only requires the simulation of two grating segments which are shifted against each other (for line edge roughness representation) or compressed/extended with respect to each other (for line width roughness representation). This way, three grating samples fabricated in silicon with dedicated line edge and line width roughness properties are measured and reconstructed in terms of the most relevant

geometrical grating parameters. The reconstruction results are compared with results extracted out of GISAXS and SEM measurements conducted by the PTB at the BESSY II synchrotron facility. All applied measurement techniques determined the grating parameters in good agreement with deviations typical below 1 nm or 1° for sidewall angles. For EUV spectrometry, simulations regarding the relative change of reflectance for a parameter variation of 0.1 nm or 0.1° around the reconstructed parameter combination show relative reflectance changes of up to 5% depending on the angle and the wavelength. These sensitivities emphasize the capability of EUV spectrometry to characterize stochastic properties of nanoscale grating structures. A more detailed analysis including multimodalities of the reconstruction results would give additional information regarding the formation of an oxide layer and could provide reliable uncertainties for each investigated parameter.

6. Mathematical Equations

$$r_{Ideal}(x,y) = \sum_{j=0}^{\infty} rect\left(\frac{x - j \cdot period}{CD}\right) \tag{2}$$

$$\begin{pmatrix} q_x \\ q_y \\ q_z \end{pmatrix} = \frac{2\pi}{\lambda}\begin{pmatrix} sin(\varphi_{out}) \cdot cos(\theta_{out}) \\ cos(\varphi_{out}) \cdot cos(\theta_{out}) - cos(\theta_{in}) \\ sin(\theta_{out}) + sin(\theta_{in}) \end{pmatrix} \tag{3}$$

7. Acknowledgements

This work was enabled by the Physikalisch-Technische Bundesanstalt which provided the samples, the reference measurements, and the primary investigation. The authors thank specially Analía Fernández Herrero for her advice in the study of roughness effects and all other contributors of the primary characterization of those samples.

8. References

[1] E. van Setten et al., "High NA EUV lithography: Next step in EUV imaging," **Proc. SPIE 10957**, 9–18 (2019).

[2] P. Thony et al., "Review of CD measurement and scatterometry," **AIP Conf Proc 683**, 381–388 (2003).

[3] B. Bunday et al., "Metrology capabilities and needs for 7nm and 5nm logic nodes," **Proc. SPIE 10145**, 102–142 (2017).

[4] A. F. Herrero, "Systematic analysis of the impact of line-edge roughness on the X-ray scattering pattern," dissertation at Technische Universität Berlin (2021).

[5] T. Itani et al., "Resist materials and processes for extreme ultraviolet lithography," *JJAP 52* (2012)

[6] A. F. Herrero, et al., "Applicability of the Debye-Waller damping factor for the determination of the line-edge roughness of lamellar gratings," *Opt. Express 27*, 32490-32507 (2019).

[7] A. Kato et al, "Analytical modeling and three-dimensional finite element simulation of line edge roughness in scatterometry," *Appl. Opt. 51*, 6457–6464 (2012).

[8] L. Bahrenberg et al., "Nanoscale grating characterization through EUV spectroscopy aided by machine learning techniques," **Proc. SPIE 11325**, 158–165 (2020)

[9] L. Bahrenberg et al., "Characterization of nanoscale gratings by spectroscopic reflectometry in the extreme ultraviolet with a stand-alone setup," *Opt. Express 28*, 20489-20502 (2020).

[10] S. Schröder et al., "Latent image characterization by spectroscopic reflectometry in the extreme ultraviolet," *JM3 21*, 021208 (2022).

[11] B. L. Henke et al., "X-ray interactions: photoabsorption, scattering, transmission, and reflection at E=50-30000 eV, Z=1-92," At. Data Nucl. Data Tables 54, 181-342 (1993).

[12] D. Attwood, "Soft x-rays and extreme ultraviolet radiation: principles and applications," Cambridge university press (2000).

[13] S. Schröder et al., "Accuracy analysis of a stand-alone EUV spectrometer for the characterization of ultrathin films and nanoscale gratings," **Proc. SPIE 11517**, 40-52 (2020).

[14] D. J. Dixit et al., "Sensitivity analysis and line edge roughness determination of 28-nm pitch silicon fins using Mueller matrix spectroscopic ellipsometry-based optical critical dimension metrology," *JM3 14*, 031208 (2015).

[15] A. F. Herrero et al., "Uncertainties in the reconstruction of nanostructures in EUV scatterometry and grazing incidence small-angle X-ray scattering," *Opt. Express 29*, 35580-35591 (2021).

[16] A. Kato, et al., "Effect of line roughness on the diffraction intensities in angular resolved scatterometry," *Appl. Opt. 49*, 6102–6110 (2010).

[17] S. Burger et al., "Benchmark of rigorous methods for electromagnetic field simulations," **Proc. SPIE 7122**, 589-600 (2008).

[18] T. Fühner et al., "Dr. LiTHO: a development and research lithography simulator," **Proc. SPIE 6520**, 1226-1237 (2007).

[19] S. Burger et al., "JCMsuite: An adaptive FEM solver for precise simulations in nano-optics," Integr. photon. nanophoton. res. appl. ITuE4 (2008).

[20] N. F. Mott, et al., "Oxidation of silicon," *Philosophical Magazine B 60*, 189-212 (1989).

BACUS N • E • W • S

Sponsorship Opportunities

Sign up now for the best sponsorship opportunities

Photomask Technology + EUV Lithography 2022
Contact: Melissa Valum, Tel: +1 360 685 5596
melissav@spie.org

Advanced Lithography + Patterning 2023
Contact: Melissa Valum, Tel: +1 360 685 5445
melissav@spie.org or Kim Abair,
Tel: +1 360 685 5499, **kima@spie.org**

Advertise in the BACUS News!

The BACUS Newsletter is the premier publication serving the photomask industry. For information on how to advertise, contact:

Melissa Valum
Tel: +1 360 685 5596
melissav@spie.org

BACUS Corporate Members

Acuphase Inc.
American Coating Technologies LLC
AMETEK Precitech, Inc.
Berliner Glas KGaA Herbert Kubatz GmbH & Co.
FUJIFILM Electronic Materials U.S.A., Inc.
Gudeng Precision Industrial Co., Ltd.
Halocarbon Products
HamaTech APE GmbH & Co. KG
Hitachi High Technologies America, Inc.
JEOL USA Inc.
Mentor Graphics Corp.
Molecular Imprints, Inc.
Panavision Federal Systems, LLC
Profilocolore Srl
Raytheon ELCAN Optical Technologies
XYALIS

Industry Briefs

The US is Spending Billions to Boost Chip Manufacturing. Will it be Enough?

Catherine Thorbecke, CNN Business

The United States government is pulling out all the stops to boost domestic semiconductor manufacturing, injecting billions of dollars into the beleaguered sector and flexing all policy muscles available to give it a leg up over competition from Asia.

When the pandemic hit in 2020, firms initially curtailed orders for these micro building blocks needed for smartphones, computers, cars, and many other products. Then, as people began working from home, demand soared for information and communication technology – and the chips that power them. A chip shortage ensued, and auto plants had to stop production because they could not obtain chips. This contributed to skyrocketing new and used vehicle prices.

Several prominent companies have announced significant investments in US manufacturing. Taiwan Semiconductor Manufacturing Company (TSMC), a powerhouse in the industry committed at least $12 billion to build a semiconductor fabrication plant in Arizona, with production expected to begin in 2024. At the start of the year, Intel said it planned to build a $20 billion semiconductor manufacturing plant in Ohio, and groundbreaking for the new chip plant took place just last month. And this month, Micron said it would invest up to $100 billion over the next two decades to build a massive semiconductor factory in upstate New York.

https://www.cnn.com/2022/10/18/tech/us-chip-manufacturing-semiconductors/index.html

Apple Freezes Plans to use China's YMTC Chips – Nikkei

Reuters

U.S. tech giant Apple has put on hold plans to use memory chips from China's Yangtze Memory Technologies Co (YMTC) in its products after Washington imposed tighter export controls against Chinese technology companies. Apple had originally planned to start using state-funded YMTC's NAND flash memory chips as early as this year. The chips were initially planned to be used only for iPhones sold in the Chinese market. The company was considering eventually purchasing up to 40% of the chips needed for all iPhones from YMTC.

The biggest implication is that it limits Apple from potentially further diversifying its supplier base by utilizing domestic China players and improving its cost profile over time.

https://www.reuters.com/technology/apple-freezes-plan-use-chinas-ymtc-chips-nikkei-2022-10-17/

ASML Shrugs off Slowdown, U.S. China Sanctions, Reports Strong Q3

Toby Sterling, Reuters

ASML Holding NV (ASML.AS), a key equipment supplier to computer chip manufacturers, reported better-than-expected third-quarter sales and profit along with record new bookings, boosting its shares. Europe's largest technology company also said it did not expect a large impact from U.S. sanctions on China. CEO Peter Wennink said customers were focused on plans to expand their long-term capacity, rather than the current economic slowdown and weakness in end-markets such as those smartphones, personal computers, or memory chips.

The overall demand for our systems continues to be strong. This resulted in record bookings in the third quarter of around 8.9 billion euros," he said in a statement. It is currently unable to keep up with demand from these companies as they are aggressively building new manufacturing plants with support from U.S. and European governments. ASML's backlog is now at 38 billion euros, and it is seeking to expand its own production capacity by 2025.

ASML shrugs off slowdown, U.S. China sanctions, reports strong Q3 | Reuters

Samsung Roadmap Includes 1.4-nm Production by 2027

Alan Patterson, EE-Times

Samsung Electronics is planning for 1.4-nm production by 2027, according to a roadmap it publicized for its chip foundry business. The company is raising the ante with top rival Taiwan Semiconductor Manufacturing Co. (TSMC) as demand for advanced semiconductors has soared. Samsung said high-performance computing (HPC), AI, 5G/6G, and automotive applications are driving demand. The technology development goal down to 1.4 nm and foundry platforms specialized for each application, together with stable supply through consistent investment, are all part of Samsung's strategy to secure. The company this year was the first to announce 3-nm production. Samsung will enhance its gate-all-around (GAA) technology with plans to introduce a 2-nm process in 2025.

Samsung Roadmap Includes 1.4-nm Production by 2027 - EE Times

Join the premier professional organization for mask makers and mask users!

About the BACUS Group

Founded in 1980 by a group of chrome blank users wanting a single voice to interact with suppliers, BACUS has grown to become the largest and most widely known forum for the exchange of technical information of interest to photomask and reticle makers. BACUS joined SPIE in January of 1991 to expand the exchange of information with mask makers around the world.

The group sponsors an informative monthly meeting and newsletter, BACUS News. The BACUS annual Photomask Technology Symposium covers photomask technology, photomask processes, lithography, materials and resists, phase shift masks, inspection and repair, metrology, and quality and manufacturing management.

Individual Membership Benefits include:

- Subscription to BACUS News (monthly)
- Eligibility to hold office on BACUS Steering Committee

spie.org/bacushome

Corporate Membership Benefits include:

- 3-10 Voting Members in the SPIE General Membership, depending on tier level
- Subscription to BACUS News (monthly)
- One online SPIE Journal Subscription
- Listed as a Corporate Member in the BACUS Monthly Newsletter

spie.org/bacushome

CALENDAR

2023

SPIE Advanced Lithography + Patterning
26 February–2 March 2023
San Jose, California, USA
www.spie.org/al

SPIE Photomask Technology and EUV Lithography
1-5 October 2023
Monterey, California, USA
www.spie.org/puv

European Mask and Lithography Conference (EMLC) 2023
19-21 June 2023
Dresden, Germany
www.emlc-conference.com

Photomask Japan (PMJ) 2023
25-27 April 2023
Online only
www.photomask-japan.org

You are invited to submit events of interest for this calendar. Please send to lindad@spie.org.

SPIE, the international society for optics and photonics, brings engineers, scientists, students, and business professionals together to advance light-based science and technology. The Society, founded in 1955, connects and engages with our global constituency through industry-leading conferences and exhibitions; publications of conference proceedings, books, and journals in the SPIE Digital Library; and career-building opportunities. Over the past five years, SPIE has contributed more than $22 million to the international optics community through our advocacy and support, including scholarships, educational resources, travel grants, endowed gifts, and public-policy development. www.spie.org.

SPIE.
International Headquarters
P.O. Box 10, Bellingham, WA 98227-0010 USA
Tel: +1 360 676 3290
Fax: +1 360 647 1445
help@spie.org • spie.org

Shipping Address
1000 20th St., Bellingham, WA 98225-6705 USA

SPIE.EUROPE
2 Alexandra Gate, Ffordd Pengam, Cardiff,
CF24 2SA, UK
Tel: +44 29 2089 4747
Fax: +44 29 2089 4750
info@spieeurope.org • spieeurope.org